Resonant excitation of injection-locked spin-torque oscillators

Ezio Iacocca[1,*] and Johan Åkerman[1,2]

[1] *Physics Department, University of Gothenburg, 412 96, Gothenburg, Sweden*
[2] *Department of Microelectronics and Applied Physics, KTH-ICT Electrum 229, 164 40, Kista, Sweden*

Theory predicts that a strongly injection-locked spin-torque oscillator (STO) should show a characteristic ringing frequency both on its approach to the locked state and under the influence of thermal noise. While experiments have so far failed to detect such ringing, we here show numerically and analytically how current modulation of injection-locked STOs can excite the ringing frequency in a resonant manner, and hence increase the experimental sensitivity. The complexity of such dynamics leads to a nonlinear resonance which can even unlock the STO as a function of the modulation strength. The results presented here offer a plausible method for experimentally measuring the ringing frequency of STOs. Moreover, the onset of unlocking also provides a measure for the maximum modulation strength that can be applied to phase-locked STOs.

I. INTRODUCTION

The theoretical prediction of the spin transfer torque (STT) effect by Slonczewski[1] and Berger[2] opened up the possibility of exciting magnetic nanostructures by means of a direct current. Particularly, stable oscillations of the magnetization can be achieved as a function of current intensity in devices known as spin-torque oscillators (STOs).[3–12] Generally, STOs are trilayered structures, or pseudo spin valves, consisting of two magnetic layers decoupled by a nonmagnetic layer. The so-called fixed layer acts as a spin polarizer for the current, while the free layer undergoes precession due to STT. STOs can also be realized using a single free layer[13,14] where STT is generated by an imbalance in spin accumulation at the two interfaces of the free layer.[15] The microwave frequencies achieved—on the order of the ferromagnetic resonance (FMR)—and the large current tunability, have led to proposed applications including microwave oscillators,[5] modulators,[16–21] spin-torque assisted MRAM,[22] logic circuits,[23] and magnonic devices.[24]

STOs are realized in two main geometries: nanosized pillars where the magnetization is assumed to precess coherently,[25] and so-called nanocontacts (NC-STO), where the current is injected in a spatially confined region (the nanocontact) while the spin valve is extended, allowing propagation of current-tuned spin-wave modes[1,3] and even generation of solitonic modes[7,8,11,26–28] and vortices.[29–31] As with other types of oscillators, several key phenomena have been experimentally demonstrated in NC-STOs, such as injection locking,[32,33] modulation,[16–18,20] and synchronization,[34,35] which in NC-STOs is mediated by propagating spin waves.

Analytically, these phenomena are studied through approximate solutions[36] of the Landau-Lifshitz-Gilbert equation extended with the Slonczewski STT term (LLGS). Such approaches have led to the fundamental understanding of the above-mentioned phenomena, such as the oscillatory approach to synchronization,[37–39] the hysteretic nature of injection locking,[40] and the origin of the nonlinear amplitude and frequency modulation (NFAM) scheme.[41,42] The cornerstone of these studies is the strong phase and power coupling of the STO, which is primarily evidenced by the oscillatory route to synchronization given by the underdamped response of a second-order differential equation. This response determines to critical figures of merit, such as a lower bound to the minimum synchronization time and an upper bound to the modulation bandwidth. Although numerical simulations have confirmed these scenarios, direct experimental proof is lacking due to the low signal-to-noise ratio and the frequency sampling limitations. However, the fundamental nature of the underdamped response suggests that it should be possible to observe at least indirectly in experiments.

In both Ref. 37 and Ref. 38, it was shown that the oscillatory route to synchronization is characterized by an eigenfrequency, or ringing frequency, Ω, damped by an exponential decay towards its injection locked steady state. Consequently, these dynamics effectively modulate the STO for a finite time (on the order of a few nanoseconds). Hence, a continuous destabilization of the injection-locked condition triggers a modulating effect that manifests itself as sidebands in the spectrum. In fact, both thermal fluctuations[38] and pulsed injection signals[37] have been shown numerically to give rise to such sidebands. These, however, had very low amplitudes, only visible due to the absence of a noise floor in the numerical simulations.

In order to observe this feature experimentally, higher output power is desired. While STOs with much higher output power can be realized using magnetic tunnel junctions (MTJs),[43–47] they also exhibit a much weaker nonlinearity,[48,49] which reduces of the ringing frequency to a few kHz at realistic, MTJ breakdown limited, injection amplitudes, and hides the ringing sidebands inside the intrinsic linewidth of these devices.

In this paper, we aim to investigate an alternative approach of resonantly exciting the ringing sidebands of an injection-locked STO, by an additional modulating current. The resulting dynamic response is however non-trivial: the injection source will attempt to keep the phase constant in time, while the modulation source induces a temporal variation of the phase (or instanta-

neous frequency). Recent experiments have shed light on the possible outcomes. For instance, mutually synchronized nanocontact STO pairs were modulated following the NFAM scheme, consistent with one equivalent oscillator.[50] However, the same authors showed that the NFAM scheme broke down in the case of *only interacting* (not mutually synchronized) nanocontact STOs. On the other hand, modulation of magnetic tunnel junction STOs has recently been shown to prevent its parametric excitation.[51] These observations suggest that modulation has a strong impact on injection-locked STOs and could very well be used to excite the ringing frequency. To explore this possibility, we investigate a nanopillar STO subject to both injection and modulation sources, by means of numerical simulations and analytical calculations. For low modulation strengths, we find that the STO is perturbed and that the ringing frequency can be *resonantly* excited. High modulation strengths, on the other hand, lead to *unlocking* of the STO. Both effects are fundamental in communication applications, where arrays of synchronized STOs are expected to act as transceivers.

The paper is divided as follows: in Section II, numerical simulations and analytical calculations are performed in the limit of low modulation strength. The excitation of the ringing frequency is shown to be resonant under both approaches. However, the analytical results are limited to a vanishingly small modulation strength. Higher modulation strengths—where the fully nonlinear problem must be solved—are numerically simulated in Section III. Here, the resonant peak undergoes a foldover, proper to nonlinear resonance. Moreover, the STO is resonantly unlocked in this regime. For yet higher, although still realistic, modulation strengths, the STO is unlocked at low frequencies. Finally, concluding remarks are provided in Section IV.

II. RESONANT EXCITATION OF THE RINGING FREQUENCY

To investigate the action of a weak modulation source on an injection-locked STO, numerical simulations of a circular nanopillar spin valve are performed in a macrospin approximation. Only the dynamics of the free layer are considered; the fixed layer is assumed to be truly static and tilted out-of-plane by an angle $\gamma_o = 30$ deg, consistent with previous studies on a similar structure.[37] The magnetization dynamics are described by the Landau-Lifshitz-Gilbert-Slonczewski (LLGS) equation:

$$\frac{d\hat{m}}{dt} = -\gamma \hat{m} \times \vec{H}_{eff} + \alpha \hat{m} \times \frac{d\hat{m}}{dt} + \alpha_J(I) \hat{m} \times \hat{m} \times \hat{M}, \quad (1)$$

where $\hat{m}$ and $\hat{M}$ are the unit vectors of the free and fixed layer magnetization, respectively. $\vec{H}_{eff}$ is the effective field including the out-of-plane external field $\mu_o H_{app} = 1.5$ T and the demagnetizing field $\mu_o M_S = 0.8$ T, where μ_o is the vacuum permeability and M_S is the saturation magnetization of the free layer. $\gamma/2\pi = 28$ GHz/T is the gyromagnetic ratio, $\alpha = 0.01$ is the Gilbert damping term, and $\alpha_J(I) = \gamma I \hbar \eta / 2\mu_o M_S e V$ is the current-dependent spin-torque magnitude, where $\hbar$ is the reduced Planck's constant, $\eta = 0.35$ is the symmetric spin-torque efficiency, e is the electron charge, and V is the volume of the fre layer. The injection and modulating currents are both added to the direct current, and hence enter the LLGS equation through $\alpha_J(I)$. Possible intermodulation effects between the sources are neglected.

The simulation is carried out in the following order: 1. The STO is driven to stable oscillations by including only the direct current $I_{dc} = 3.5$ mA for 20 ns. For this choice of parameters, the STO precesses at $\omega/2\pi = 24.27$ GHz; 2. The injection current, $I_{ac} = \mu_{inj} I_{dc} \cos \omega_e t$ is added at the STO free-running frequency, i.e., $\omega_e = \omega$. The ratio μ_{inj} quantifies the injection strength and is considered a free parameter. This regime is sustained for 100 ns to ensure proper convergence to an injection-locked state; 3. Finally, the modulation current is added as $I_m = \mu_m I_{dc} \cos \omega_m t$, similarly to the experimental procedure.[16] The modulation frequency, $\omega_m/2\pi$, is swept between 20 and 1000 MHz in steps of 20 MHz. For each $\omega_m/2\pi$ value, the simulation is run for 100 ns. Its FFT is calculated using a Hann window and zero padding to achieve a frequency resolution of 9.5 MHz.

From the FFTs, we extract the power of the first modulation sideband as a function of $\omega_m/2\pi$ (shown by the blue line in Fig. 1.a, for $\mu_m = 0.005$ and $\mu_{inj} = 0.1369$). Interestingly, the sideband power peaks at a particular frequency, denoted $\omega_{max}/2\pi$. Repeating the same procedure for weaker μ_{inj} (dashed lines in Fig. 1.a) shifts $\omega_{max}/2\pi$ to lower frequencies. This shift can be visualized by plotting $\omega_{max}/2\pi$ as a function of μ_{inj}, shown by the blue circles in Fig. 1.b and resembles the ringing frequency-dependence derived in Ref. 37 (black dashed line), in particular in the square-root dependence and the existence of a critical injection strength, $\mu_{cr,1}$. However, $\mu_{cr,1}$ is higher than the ideal case, denoted as μ_{cr} in the same figure. Moreover, repeating the simulation for a higher modulation strength, $\mu_m = 0.01$, reveals yet a different critical injection strength, $\mu_{cr,2} > \mu_{cr,1}$ i.e., μ_{cr} is a function of μ_m.

In order to shed light on the results in Fig. 1.b, analytical calculations are performed in the framework of the auto-oscillator equation proposed by Slavin and Tiberkevich[36]. Considering both an injection and a modulating source, one can write the auto-oscillator equation as

$$\frac{dc}{dt} + i\omega(|c^2|)c + (\Gamma_+(|c^2|) - \Gamma_-(I(t), |c^2|))c = f e^{i\omega_e - i\phi}. \quad (2)$$

Here c is the complex oscillation amplitude, so $p = |c^2|$ is its power, ω is the free-running STO frequency, and Γ_+ and Γ_- map the Gilbert damping and STT term, respectively. The modulation source is considered a slow time scale, and is thus included in the STT term as a

time-dependent current $I(t)$:

$$I(t) = I_{dc}(1 + \mu_m \cos\omega_m t). \tag{3}$$

The injection source has the same time scale as ω, and so is included in Eq. (2) as a perturbative term[36], where $f \propto \mu_{inj} \tan\gamma_o$ (See Ref. 26) is the injection power, ω_e is the frequency of the injection source, and ϕ its phase relative to the STO frequency.

A set of coupled equations are obtained from Eq. (2) and solved by a Fourier expansion method.[42] To this end, we assume that the STO is injection-locked. We hence linearize Eq. (2) about the *injection-locked* conditions, $(\delta p_0, \phi_0)$.[37] The resulting set of equations is given by

$$\frac{d\delta p}{dt} = K_1 \cos\omega_m t - K_2\phi - [K_3 + K_4 \cos\omega_m t]\,\delta p, \tag{4a}$$

$$\frac{d\phi}{dt} = K_5\delta p + K_6\phi, \tag{4b}$$

where the coefficients are given by:

$$K_1 = \xi\Gamma_G(1 - p_{0f})\mu_m, \tag{5a}$$

$$K_2 = F\sin\phi_0, \tag{5b}$$

$$K_3 = 2\Gamma_p - F\cos\phi_0, \tag{5c}$$

$$K_4 = 2\xi\Gamma_G(2p_{0f} - 1)\mu_m, \tag{5d}$$

$$K_5 = 2\nu\Gamma_p - F\sin\phi_0, \tag{5e}$$

$$K_6 = -F\cos\phi_0. \tag{5f}$$

Here, $p_{0f} = (\xi - 1)/(\xi + Q)$ is the free-running power, Q is the nonlinear damping coefficient, $\xi = I_{dc}/I_{th}$ is the supercriticality, I_{th} is the threshold current for oscillations, $\Gamma_G = \alpha\omega_o$ is the damping, ω_o is the FMR frequency, $F = f/\sqrt{p_{0f}}$ is the normalized injection power, ν is the nonlinearity coefficient, and Γ_p is the restoration rate. The approximation $\delta p \ll p_{0f}$ was used in Eq. (4) in order to obtain an analytically tractable result. Note also that the nonlinear terms in Eq. 4a must be kept in order to reproduce the correct modulated spectrum.[17,41,42]

The set of Eqs. (4) have solutions in the form of Fourier series, both in power and in phase. These solutions indicate that the injection-locked STO is indeed modulated by the slow time-varying current. As discussed in Ref. 42, the exact solution is given by an infinite matrix of coupled coefficients. However, a good approximation can be obtained by recursively generating the Fourier coefficients due to their harmonic-dependent factorial decay. In this framework, the first harmonic coefficient, A_1 [Eq. (A2a)] is proportional to the modulation strength (see Appendix A), and can be analytically calculated. We are interested in the frequency dependence of the maximum STO power. Here, we assume that the STO is injection-locked in the non-Adlerian regime. Furthermore, it is assumed that the frequency mismatch is vanishingly small ($\Delta\omega \to 0$) and the modulation strength fulfills the condition $K_4(\mu_m) \ll \Gamma_p$ i.e., the modulation-induced fluctuations are strongly damped by the STO. The range of validity for such approximations is discussed below. The maximum power calculated from Eq. (A1a) is then given by

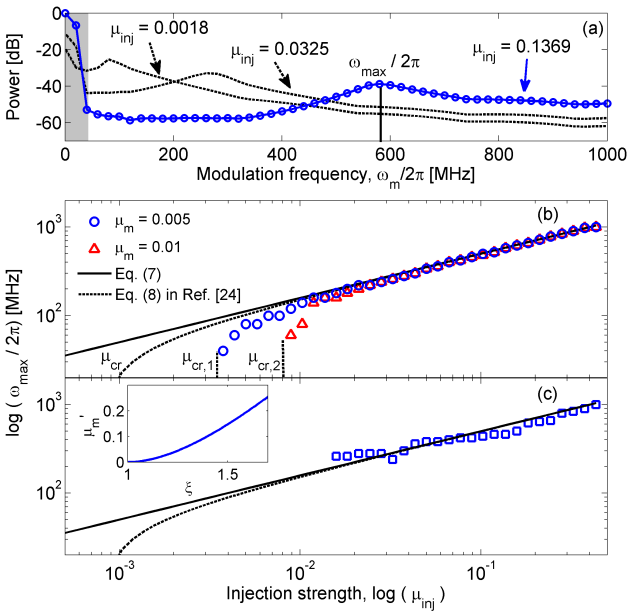

FIG. 1. (a) Maximum sideband power as a function of the modulation frequency, $\omega_m/2\pi$ for several values of μ_{inj}. In each case, a peak at a particular frequency is observed ($\omega_{max}/2\pi$ for the blue line). This peak marks the resonance of the STO ringing frequency due to the modulation source. As the modulation frequency approaches 0, a step is observed, due to frequency leakage originating from the main oscillation peak. (b-c) $\omega_{max}/2\pi$ as a function of μ_{inj} for representative values of the modulation strength. In (b), the low modulation strengths give good agreement between the simulations (circles and triangles) and the analytical estimates (solid and dashed lines). (c) The agreement is lost when $\mu_m > \mu'_m$ and the analytical agreement is only qualitative. The inset shows the maximum modulation, μ'_m, as a function of the supercriticality at which Eq. (7) is still valid.

$$\delta p_{max} = \frac{K_1\omega_m}{\sqrt{(\omega_m^2 - K_2K_5)^2 + K_3^2\omega_m^2}}. \tag{6}$$

The form of Eq. (6) is resonant *only* as a function of ω_m and it peaks at a frequency ω_{max}, given by

$$\omega_{max} = \Gamma_p\sqrt{\frac{\mu_{inj}}{\mu_{cr}}}, \tag{7}$$

where $\mu_{cr} = F_{cr}2\sqrt{2p_{0f}}(\xi - 1)/\Gamma_p \tan\gamma_o$ is the critical strength for non-Adlerian dynamics and $F_{cr} = \Gamma_p/(2\nu\sin\phi_0)$ as derived in Ref. 37. Due to the approximations made, Eq. (7) agrees asymptotically with the simulation results, as shown by the solid black line in Fig. 1.b. This is an indication of the highly nonlinear dynamics occurring in the system. However, the analytical result of Eq. (7) allows to conclude that the features observed in Fig. 1 stem from the resonant excitation of the ringing frequency due to a perturbative modulation

source. This conclusion is central to this work as it indicates that modulation not only perturbs the injection-locked state, but can also lead to a substantial power - phase variation that eventually breaks the injection locking, as discussed in the next section.

The analytical formulation breaks down when the approximations on the smallness of μ_m and δp are no longer satisfied. We here discuss the range of validity of such approximations given the dynamics of the system. First, the resonant condition implies a correlated increase in the power and phase variation. Naturally, the condition $\delta p \ll p_{0f}$ might not be satisfied in such a case. Expressing Eq. (6) as a function of the STO free-running parameters by use of Eq. (5) leads to

$$\delta p_{max}(\omega = \omega_{max}) = \frac{\xi}{\xi - 1}(1 - p_{0f})\frac{\mu'_m}{2}. \qquad (8)$$

Under the simulation conditions specified above, $\delta p_{max}(\omega = \omega_{max}) \approx p_{0f}$ when $\mu'_m \approx 0.04$, which experimentally is a small quantity. On the other hand, the condition of negligible modulation $K_4(\mu_m) \ll \Gamma_p$ is necessary to obtain a closed form for A_1 (see Appendix A) and obtain Eq. (8). Consequently, this approach fails to describe the influence of μ_m on μ_{cr}.

For non-negligible μ_m, the linearization applied to obtain Eq. (4) is no longer a good approximation, and the full nonlinear equations should be used. This can be seen in Fig. 1.c, where ω_{max} is shown as a function of μ_{inj} when $\mu_m = 0.05$. Clearly, both analytical equations cannot describe the fine features obtained from the numerical results. This fact imposes the main limitation of the present analytical approach.

Noteworthy, Eq. (8) suggests that the maximum modulation strength, μ'_m, can be enhanced as a function of the direct current, as shown in the inset of Fig. 1.c. However, the larger precession angles excited as $\xi = I_{dc}/I_{th}$ increases can fall outside the validity range of the auto-oscillator equation, Eq. (2).

An alternative analytical approach suggested by Serpico and co-authors[38,40] provides the advantage of supporting large amplitude magnetization precession. From this point of view, such an approach could provide a better description of the observed resonant ringing and, arguably, of the results described in the following section. However, a description of the modulation in such a framework is lacking, and its detailed study is required in order to reveal its limitations. On the other hand, the slow time-scale nonlinearity introduced by the modulation term also suggests an approximate analytical solution. Consequently, a numerical description is preferred to overcome the abovementioned limitations, as discussed in the next section.

III. MODULATION-MEDIATED UNLOCKING

For modulation strengths such that $\delta p_{max}(\omega = \omega_{max}) \approx p_{0f}$, the auto-oscillator equation Eq. (2) can no longer be linearized. Consequently, nonlinear effects dominate this regime, leading mainly to the unlocking of the STO. In the following, we study these effects by performing macrospin simulations spanning both μ_m and ω_m.

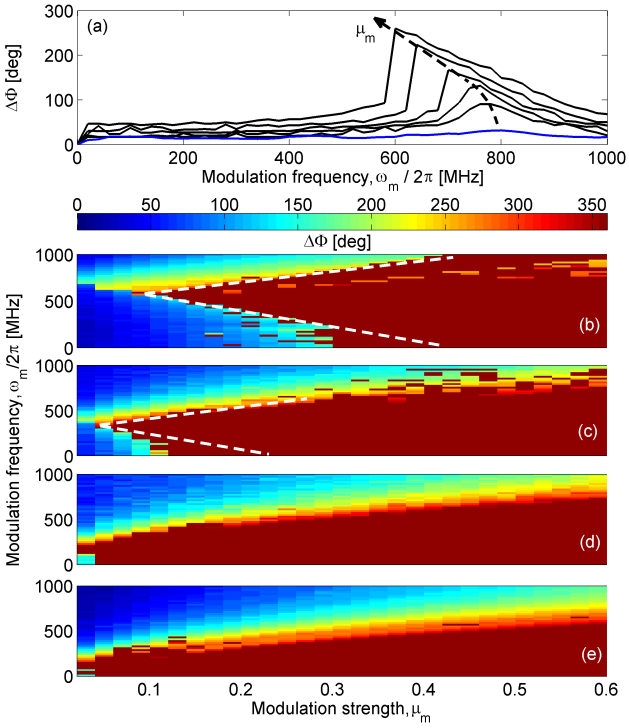

FIG. 2. (a) Foldover observed in the resonant peak as a function of μ_m. This effect is proper to nonlinear resonance. Maps of the maximum phase difference, $\Delta\Phi$, between the injection signal and the STO time trace for (b) $\mu_{inj} = 0.2812$, (c) $\mu_{inj} = 0.1$, (d) $\mu_{inj} = 0.03$, and (e) $\mu_{inj} = 0.01$. In (b), the STO is resonantly unlocked for $\mu_m < 0.3$. The enhancement of the unlocked region is stressed with white dashed lines. When $\mu_m > 0.3$ the STO is unlocked via modulated unlocking. As the injection strength is reduced, the phase-locking bandwidth also decreases and the modulated unlocking progressively dominates the maps, as observed from (c) to (e).

First, we consider the case where μ_m is close to the negligible δp condition. To this end, μ_m is swept from 0.03 to 0.1 in steps of 0.01. For each value of μ_m, $\omega_m/2\pi$ is swept back and forth between 1000 and 0 MHz in steps of 20 MHz. We consider a rather strong injection strength of $\mu_1 = 0.2812$, for which the ringing frequency is $\Omega_1 \approx 840$ MHz. The parameter we are interested in is the maximum phase deviation, $\Delta\Phi$, between the STO and the pure injection signal which is obtained by determining the phase difference between the STO and the injection source for each period, $\Phi(t)$, and then calculating $\Delta\Phi = |\max(\Phi(t)) - \min(\Phi(t))|$. This method is sensitive to the sampling time used in the simulation, here set to 2 ps, which introduces a maximum error of ≈ 10 deg.

Stemming from the STO's power - phase coupling, the

quantity $\Delta\Phi$ maps the features of δp_{max}, Eq. (6). At the same time, $\Delta\Phi$ can be used to conveniently describe the STO state. An injection-locked condition is defined when $\Delta\Phi$ is bounded, i.e. when its value lies between 0 and 360 deg. Note that this definition considers the pulling regime[39] as an unlocked state.

The quantity $\Delta\Phi$ as a function of ω_m and μ_m is shown in Fig. 2.a. Here, the blue line indicates the case where $\mu_m = 0.03$ and the approximations discussed in the previous section hold. As μ_m increases, $\Delta\Phi$ becomes progressively asymmetric, and is accompanied by a shift in the resonance frequency (dashed line). Such a response is known as a foldover, and is proper to nonlinear resonant processes such as spin wave excitations in a thin film.[52] This response arises *only* as a function of μ_m, and is hence related to the carrier frequency shift observed in modulated STOs.[17,41,42]

Further increasing μ_m leads to a point where $\Delta\Phi$ becomes unbounded, marking the unlocking of the STO. This can be visualized in the color map of Fig. 2.b, both as a function of μ_m and of ω_m, where μ_m is swept from 0.03 to 0.6 in steps of 0.02. The color scheme is bounded to 360 deg, so that the maximum (deep red) indicates the unlocked region. Since the results for the frequency sweeps did not show appreciable hysteresis, we limit the following discussion to decreasing frequencies, consistent with experimental procedures.[51]

We can identify two different mechanisms for modulation-mediated unlocking. First, in the region spanning $0.1 < \mu_m < 0.3$, unlocking occurs as $\Delta\Phi$ surpasses the bounded condition, while it is otherwise locked. Alternatively, one can envision that a strong variation in $\Phi(t)$ leads to an instantaneous frequency, $d\Phi(t)/dt$, that surpasses the locking range, and hence unlocks the STO. Indeed, Fig. 2.b shows that the unlocked region widens as μ_m increases (white dashed lines), in agreement with the resonance enhancement shown in Fig. 2.a. Consequently, we refer to this regime as *resonant unlocking*. Secondly, in the region $\mu_m > 0.3$, the STO is *always* unlocked at low frequencies. A qualitative understanding of this feature comes from the fact that a slow modulation, $\omega_m \to 0$, can be considered a direct current on the STO timescale. Then, a frequency mismatch between the STO and the injection source must be defined and the locking condition will be given by the familiar locking range. We refer to this mechanism as *non-resonant unlocking*.

The previous results were obtained under a rather large injection strength. However, the unlocking mechanisms discussed above also exist for lower injection strengths. The maps of Fig. 2.c-e illustrate the progressive increase of the non-resonant unlocking region as the injection strength decreases, namely, $\mu_{inj} = 0.1$, $= 0.03$, and 0.01. Note that the ringing frequency also changes to values 500, 300, and 100 MHz, respectively. The fact that the non-resonant unlocking dominates the map is again understood from the locking range at lower injection strength, consistent with the previous discussion.

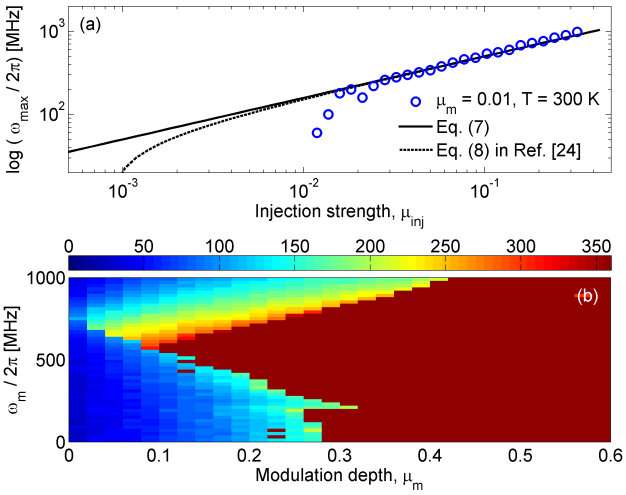

FIG. 3. (a) $\omega_{max}/2\pi$ as a function of μ_{inj} for $\mu_m = 0.01$. The inclusion of thermal fluctuations does not affect the agreement with the analytical estimates (solid and dashed lines). (b) Map of the maximum phase difference, $\Delta\Phi$, with the same parameters as used for Fig. 2.b. Here the thermal fluctuations lead to a smoother map, preventing the pulled regime from being numerically considered locked and reducing the numerical artifacts at low frequencies.

Interestingly, the non-resonant unlocking also exhibits a dependence on the modulation frequency. Qualitatively, this dependence is related to the limited synchronization time of the STO,[37] which defines a modulation bandwidth.[42] When the modulation frequency surpasses the modulation bandwidth, the STO is no longer effectively modulated, and its phase is less and less perturbed by the modulating signal.

We would like to stress that the mapping of $\Delta\Phi$ shows a few isolated points where the dynamics are quantified as unlocked, as well as apparent bistable states. These features are artifacts of the zero-temperature simulations. Closer inspection of the time traces reveals both numerical phase slips and absence of phase slips during the pulling regime. In order to prevent these artifacts, a thermal field was included in the modelling, following Brown's description.[53] The amplitude of the thermal field is given by appropriately scaling[54] an equivalent temperature of 300 K. Fig. 3.a shows $\omega_{max}/2\pi$ as a function of μ_{inj} along with the analytical estimates. Similarly to Fig. 1.b, the ringing frequency is well reproduced. We argue that the resonant character of the excitation makes it robust to thermal fluctuations in the system. The map of $\Delta\Phi$ is shown in Fig. 3.b for the same parameters used for Fig. 2.b. As expected, the general features of the map are conserved, such as the existence of regions of resonant and non-resonant unlocking. In contrast, the apparent bistability is completely absent.

IV. CONCLUSION

We have studied modulation of injection-locked STOs both analytically and numerically. It was found that the modulation is capable of resonantly exciting the STO, leading to enhanced sideband power and even to the unlocking of the STO. These features arise as a result of the competition between modulation and injection; the modulation tries to vary the STO frequency, while the injection tries to keep it fixed. The fundamental properties of STOs may be probed using these effects. For instance, the ringing frequency could be mapped by the resonant condition of the modulating sidebands. On the other hand, the STO modulation bandwidth could be mapped by measuring the maximum frequency at a given μ_m and μ_{inj} for non-resonant unlocking. We believe that this features provides insight on the modulation of synchronized STO pairs. In fact, the presented results imply that the maximum modulation strength in such a device would be limited by the coupling strength between the STOs.

The authors acknowledge P.K. Muduli, Ye. Pogoryelov, and P. Dürrenfeld for fruitful discussions. Support from the Swedish Research Council (VR) is gratefully acknowledged. Johan Åkerman is a Royal Academy of Sciences Research Fellow supported by a grant from the Knut and Alice Wallenberg Foundation.

Appendix A

The solution to Eq. (4) is given by the Fourier series of power and phase

$$\delta p = A_0 + \sum_{n=1}^{\infty} A_n \sin n\omega_m t + B_n \cos n\omega_m t, \quad \text{(A1a)}$$

$$\phi = C_0 + \sum_{n=1}^{\infty} C_n \sin n\omega_m t + D_n \cos n\omega_m t. \quad \text{(A1b)}$$

Following the procedure of Ref. 42, it is possible to insert Eq. (A1) into Eq. (4) and rearrange in harmonic coefficients. Similarly, each coefficient will be inversely proportional to $(n\omega_m)^2$, so we can approximate the solution by neglecting coefficients with $n > 2$. The resulting equations for A_1 and $B1$ are

$$A_1 \left[\omega_m I_1 + \frac{H_1}{\omega_m I_1}\left(H_1 - \frac{K_4^2}{2H_0}\right) + \frac{(K_4/2)^2}{2\omega_m I_2}\right] = K1, \quad \text{(A2a)}$$

$$B_1 = \frac{H_1 A_1}{\omega_m^2 + K_6^2}. \quad \text{(A2b)}$$

where

$$H_1 = K3 - \frac{K_2 K_5 K_6}{\omega_m^2 + K_6^2}, \quad \text{(A3a)}$$

$$I_1 = 1 - \frac{K_2 K_5}{\omega_m^2 + K_6^2}, \quad \text{(A3b)}$$

(A3c)

Neglecting the K_4 terms in Eq. (A2a) ($K_4 \ll \Gamma_p$) and K_6 ($\Delta\omega \to 0$) leads to a closed form for A_1, which can be maximized to obtain Eq. (6).

* ezio.iacocca@physics.gu.se

[1] J. C. Slonczewski, Journal of Magnetism and Magnetic Materials **159**, L1 (1996).
[2] L. Berger, Phys. Rev. B **54**, 9353 (1996).
[3] W. H. Rippard, M. R. Pufall, S. Kaka, S. E. Russek, and T. J. Silva, Phys. Rev. Lett. **92**, 027201 (2004).
[4] W. H. Rippard, M. R. Pufall, S. Kaka, T. J. Silva, and S. E. Russek, Phys. Rev. B **70**, 100406 (2004).
[5] T. Silva and W. Rippard, Journal of Magnetism and Magnetic Materials **320**, 1260 (2008).
[6] S. Bonetti, P. Muduli, F. Mancoff, and J. Åkerman, Applied Physics Letters **94**, 102507 (2009).
[7] S. Bonetti, V. Tiberkevich, G. Consolo, G. Finocchio, P. Muduli, F. Mancoff, A. Slavin, and J. Åkerman, Phys. Rev. Lett. **105**, 217204 (2010).
[8] M. Madami, S. Bonetti, G. Consolo, S. Tacchi, G. Carlotti, G. Gubbiotti, F. B. Mancoff, M. A. Yar, and J. Åkerman, Nature Nanotechnology **6**, 635 (2011).
[9] S. R. Sani, J. Persson, S. M. Mohseni, V. Fallahi, and J. Åkerman, Journal of Applied Physics **109**, 07C913 (2011).
[10] S. M. Mohseni, S. R. Sani, J. Persson, T. N. Anh Nguyen, S. Chung, Y. Pogoryelov, and J. Åkerman, Physica Status Solidi RRL **5**, 432 (2011).
[11] S. Bonetti, V. Puliafito, G. Consolo, V. S. Tiberkevich, A. N. Slavin, and J. Åkerman, Phys. Rev. B **85**, 174427 (2012).
[12] J. Persson, S. R. Sani, S. Bonetti, F. Magnusson, Y. Pogoryelov, S. M. Mohseni, S. Gunnarsson, M. Norling, C. Stoij, and J. Åkerman, IEEE Trans. Magn. **48**, 07C913 (2012).
[13] B. Özyilmaz, A. D. Kent, J. Z. Sun, M. J. Rooks, and R. H. Koch, Phys. Rev. Lett. **93**, 176604 (2004).
[14] S. R. Sani, P. Dürrenfeld, S. M. Mohseni, S. Chung, and Å, IEEE Trans. Magn. **in press** (2013).
[15] M. L. Polianski and P. W. Brouwer, Phys. Rev. Lett. **92**, 026602 (2004).
[16] M. R. Pufall, W. H. Rippard, S. Kaka, T. J. Silva, and S. E. Russek, Applied Physics Letters **86**, 082506 (2005).
[17] P. K. Muduli, Y. Pogoryelov, S. Bonetti, G. Consolo, F. Mancoff, and J. Åkerman, Phys. Rev. B **81**, 140408 (2010).
[18] Y. Pogoryelov, P. K. Muduli, S. Bonetti, E. Iacocca, F. Mancoff, and J. Åkerman, Applied Physics Letters **98**, 192501 (2011).

[19] P. Muduli, Y. Pogoryelov, F. Mancoff, and J. Åkerman, Magnetics, IEEE Transactions on **47**, 1575 (2011).

[20] M. Manfrini, T. Devolder, J.-V. Kim, P. Crozat, C. Chappert, W. V. Roy, and L. Lagae, Journal of Applied Physics **109**, 083940 (2011).

[21] Y. Pogoryelov, P. K. Muduli, and J. Åkerman, IEEE Trans. Magn. **48**, 4077 (2012).

[22] J. Katine and E. E. Fullertonh, Journal of Magnetism and Magnetic Materials **320**, 1217 (2008).

[23] F. Macià, A. D. Kent, and F. C. Hoppensteadt, Nanotechnology **22**, 095301 (2011).

[24] S. Bonetti and J. Åkerman, in *Magnonics*, Topics in Applied Physics, Vol. 125, edited by S. O. Demokritov and A. N. Slavin (Springer Berlin Heidelberg, 2013) pp. 177–187.

[25] S. I. Kiselev, J. C. Sankey, I. N. Krivorotov, N. C. Emley, R. J. Schoelkopf, R. A. Buhrman, and D. C. Ralph, Nature **425**, 380 (2003).

[26] A. Slavin and V. Tiberkevich, Phys. Rev. Lett. **95**, 237201 (2005).

[27] S. M. Mohseni, S. R. Sani, J. Persson, T. N. A. Nguyen, S. Chung, Y. Pogoryelov, P. K. Muduli, E. Iacocca, A. Eklund, R. K. Dumas, S. Bonetti, A. Deac, M. A. Hoefer, and J. Åkerman, Science **339**, 1295 (2013), http://www.sciencemag.org/content/339/6125/1295.full.pdf.

[28] E. Iacocca, R. Dumas, L. Bookman, S. M. Mohseni, S. Chung, M. Hoefer, and J. Åkerman, In preparation (2013).

[29] M. R. Pufall, W. H. Rippard, M. L. Schneider, and S. E. Russek, Phys. Rev. B **75**, 140404 (2007).

[30] Q. Mistral, M. van Kampen, G. Hrkac, J.-V. Kim, T. Devolder, P. Crozat, C. Chappert, L. Lagae, and T. Schrefl, Phys. Rev. Lett. **100**, 257201 (2008).

[31] S. Petit-Watelot, A. Kim, Joo-Von Ruotolo, R. M. Otxoa, K. Bouzehouane, J. Grollier, A. Vansteenkiste, B. Van de Wiele, V. Cros, and T. Devolder, Nature Physics (2012), 10.1038/nphys2362.

[32] W. H. Rippard, M. R. Pufall, S. Kaka, T. J. Silva, S. E. Russek, and J. A. Katine, Phys. Rev. Lett. **95**, 067203 (2005).

[33] B. Georges, J. Grollier, M. Darques, V. Cros, C. Deranlot, B. Marcilhac, G. Faini, and A. Fert, Phys. Rev. Lett. **101**, 017201 (2008).

[34] S. Kaka, M. R. Pufall, W. H. Rippard, T. J. Silva, S. E. Russek, and J. A. Katine, Nature **437**, 389 (2005).

[35] M. R. Pufall, W. H. Rippard, S. E. Russek, S. Kaka, and J. A. Katine, Phys. Rev. Lett. **97**, 087206 (2006).

[36] A. Slavin and V. Tiberkevich, Magnetics, IEEE Transactions on **45**, 1875 (2009).

[37] Y. Zhou, V. Tiberkevich, G. Consolo, E. Iacocca, B. Azzerboni, A. Slavin, and J. Åkerman, Phys. Rev. B **82**, 012408 (2010).

[38] M. d'Aquino, C. Serpico, R. Bonin, G. Bertotti, and I. D. Mayergoyz, Phys. Rev. B **82**, 064415 (2010).

[39] E. Iacocca and J. Åkerman, Journal of Applied Physics **110**, 103910 (2011).

[40] C. Serpico, R. Bonin, G. Bertotti, M. D'Aquino, and I. D. Mayergoyz, IEEE Transactions on Magnetics **45**, 3441 (2009).

[41] G. Consolo, V. Puliafito, G. Finocchio, L. Lopez-Diaz, R. Zivieri, L. Giovannini, F. Nizzoli, G. Valenti, and B. Azzerboni, Magnetics, IEEE Transactions on **46**, 3629 (2010).

[42] E. Iacocca and J. Åkerman, Phys. Rev. B **85**, 184420 (2012).

[43] A. V. Nazarov, K. Nikolaev, Z. Gao, H. Cho, and D. Song, Journal of Applied Physics **103**, 07A503 (2008).

[44] A. M. Deac, A. Fukushima, H. Kubota, H. Maehara, Y. Suzuki, S. Yuasa, Y. Nagamine, K. Tsunekawa, D. D. Djayaprawira, and N. Watanabe, Nature Physics **4**, 803 (2008).

[45] D. Houssameddine, S. H. Florez, J. A. Katine, J.-P. Michel, U. Ebels, D. Mauri, O. Ozatay, B. Delaet, B. Viala, L. Folks, B. D. Terris, and M.-C. Cyrille, Applied Physics Letters **93**, 022505 (2008).

[46] P. K. Muduli, O. G. Heinonen, and J. Åkerman, Phys. Rev. B **83**, 184410 (2011).

[47] P. K. Muduli, O. G. Heinonen, and J. Åkerman, Phys. Rev. Lett. **108**, 207203 (2012).

[48] L. Bianchini, S. Cornelissen, J.-V. Kim, T. Devolder, W. van Roy, L. Lagae, and C. Chappert, Applied Physics Letters **97**, 032502 (2010).

[49] M. Quinsat, D. Gusakova, J. F. Sierra, J. P. Michel, D. Houssameddine, B. Delaet, M.-C. Cyrille, U. Ebels, B. Dieny, L. D. Buda-Prejbeanu, J. A. Katine, D. Mauri, A. Zeltser, M. Prigent, J.-C. Nallatamby, and R. Sommet, Applied Physics Letters **97**, 182507 (2010).

[50] Y. Pogoryelov, P. K. Muduli, S. Bonetti, F. Mancoff, and J. Åkerman, Applied Physics Letters **98**, 192506 (2011).

[51] P. Dürrenfeld, E. Iacocca, P. K. Muduli, and J. Åkerman, In preparation.

[52] D. Stancil and A. Prabhakar, *Spin waves: Theory and applications* (Springer, 2009).

[53] W. F. Brown, Phys. Rev. **130**, 1677 (1963).

[54] M. d'Aquino, C. Serpico, G. Coppola, I. D. Mayergoyz, and G. Bertotti, Journal of Applied Physics **99**, 08B905 (2006).